Lange, D., Tilmann, F., Rietbrock, A., Collings, R., Natawidjaja, D. H., Suwargadi, B. W., Barton, P., Henstock, T., Ryberg, T. (2010): The Fine Structure of the Subducted Investigator Fracture Zone in Western Sumatra as Seen by Local Seismicity. - Earth and Planetary Science Letters, 298, 1-2, 47-56

DOI: 10.1016/j.epsl.2010.07.020

The Fine Structure of the Subducted Investigator Fracture Zone in Western Sumatra as Seen by Local Seismicity

Dietrich Lange[a], Frederik Tilmann[a], Andreas Rietbrock[b], Rachel Collings[b], Danny H. Natawidjaja[c], Bambang W. Suwargadi[c], Penny Barton[a], Timothy Henstock[d], Trond Ryberg[e],

[a]*Department of Earth Sciences, University of Cambridge, United Kingdom.*
[b]*University of Liverpool, United Kingdom.*
[c]*LabEarth, Indonesian Institute of Sciences (LIPI).*
[d]*National Oceanography Centre, Southampton, United Kingdom.*
[e]*GFZ Potsdam, Germany.*

Abstract

The Sumatran margin suffered three great earthquakes in recent years (Aceh-Andaman 26 December 2004 Mw=9.1, Nias 28 March 2005 Mw=8.7, Bengkulu 12 September 2007 Mw=8.5). Here we present local earthquake data from a dense, amphibious local seismic network covering a segment of the Sumatran margin that last ruptured in 1797. The occurrence of forearc islands along this part of the Sumatran margin allows the deployment of seismic land-stations above the shallow part of the thrust fault. In combination with ocean bottom seismometers this station geometry provides high quality hypocentre location for the updip end of the seismogenic zone in an area where geodetic data are also available. In this region, the Investigator Fracture Zone (IFZ), which consists of 4 sub-ridges, is subducted below the Sunda plate. This topography appears to influence seismicity at all depth intervals. A well-defined linear streak of seismicity extending from 80 to 200 km depth is lying along the prolongation of closely spaced IFZ sub-ridges. More intermediate depth seismicity is located to the southeast this string of seismicity and is related to subducted rough oceanic seafloor. The plate interface beneath Siberut Island which ruptured last in 1797 is characterised by almost complete absence of seismicity.

Keywords: Local Seismicity, Subduction Zone, Ridge subduction, Sumatra,

1. Introduction

Subducted seamounts and ridge systems have been thought to influence the rupture behavior of major earthquakes (Abercrombie et al., 2001; Bilek et al., 2003). Brittle seismogenic rupture of large faults can be stalled (Robinson et al., 2006; Gahalaut et al., 2010) or inhibited by subducted fracture zones and seamounts (Kodaira et al., 2000). Some authors have proposed enhanced coupling over subducted seamounts (e.g. Scholz and Small, 1997; Park et al., 2004) while recent studies propose weak coupling associated with incoming plate relief (Mochizuki et al., 2008; Sparkes et al., 2009). For the South American subduction zone, Kirby et al. (1996) observed that intermediate earthquakes often occur in roughly linear clusters that connect at the surface to incoming plate heterogeneities, such as coastal embayments and offshore seamounts. In Sumatra, the oceanic Indo-Australian plate subducts obliquely beneath the Eurasian plate (Figure 1). A ~2500 km long, NS trending topographic feature, the Investigator Fracture zone (IFZ), is situated on the incoming Indo-Australian plate. The oceanic plate west of the IFZ is significantly younger, the age contrast relative to the eastern side being up to ~15 Ma (Müller et al., 1997). The IFZ is subducted at an oblique angle of ~65° and a velocity of 57 mm/yr below the Sumatran mainland, and the direction of the fracture zone trend near the trench is almost parallel to the convergence vector. Just before the trench the IFZ consists of 4 individual ridges, which migrate northwards along the Sumatran margin and lead to kinks in the trend of the deformation front (Kopp et al., 2008). Isolated seamounts are situated on top of the ridges as well as on their flanks (Kopp et al., 2008).

The Sumatran margin has been the site of a number of great earthquakes in the recent past (Figure 1): The regions north of Nias ruptured in 2004 (e.g. Krüger and Ohrnberger, 2005) and 2005 (Konca et al., 2007), and the region south of Siberut ruptured partially in 2007 (Konca et al., 2008). There remains an unruptured segment between the sites of these great earthquakes which is located below Siberut Island. This segment ruptured last in 1797 (Newcomb and McCann, 1987; Natawidjaja et al., 2006) and is known to be strongly coupled from GPS and coral data (Chlieh et al., 2008). The 12 September 2007 earthquake only partially ruptured the 1833 earthquake region, the total slip deficit below Siberut and the Pagai Islands since the large ruptures from 1797 and 1833 is approximately 8 m, equivalent to a moment deficit corresponding to an M_w=8.8 earthquake (Sieh et al., 2008). Therefore, the segment is in an advanced stage of the seismic cycle (Konca et al., 2008).

Here, we use high-resolution local observations from an amphibious network of seismometers in the region where the IFZ subducts below the Sumatran mainland to characterise the lateral change of seismicity, and relate the intermediate and shallow seismicity to the structure of the incoming oceanic plate. The serendipitous occurrence of forearc islands along this part of the Sumatran margin allows the deployment of seismic land-stations above the shallow part of the thrust fault. These island stations, together with ocean bottom seismometers (OBS), provide high quality locations for the up-dip end of the seismogenic zone where the coupling of the plate interface is known (Chlieh et al., 2008; Prawirodirdjo et al., 2010).

2. Experiment and Data

A dense seismic network was installed along the west Sumatran margin in April 2008 between 1.8°S and 1.8°N (Figure 2). The land network comprised 52 continuously recording three component stations running at 50 and 100 Hz, including 7 broadband stations. To improve resolution of the offshore part the network was complemented by 10 three-component ocean bottom seismometers with differential pressure gauge channel (OBS) in June 2008. During October 2008, 10 stations were removed from the Sumatran mainland such that 42 land-stations (short period: 34; 7 broadband) and 10 OBS stations remained until February 2009. In addition to the temporary deployment we included the data from 8 permanent stations operated by BMG and 2 permanent stations operated by GEOFON in the analysis. For strong and deep events we incorporated the data from a temporary deployment of 39 stations to the north of our deployment (GFZ network) and 27 stations from an adjacent temporary network to the south (Mentawai stations, Collings et al., 2009). For the time span of 14 days between 25 May and 10 June 2008 the data from an active experiment comprising 46 OBS stations were also included into this study. Table ST1 summarizes the networks and instruments used for the study.

3. Data Processing and Inversion for 1-D velocity model

Event detection was carried out on the continuous data using a grid search in time and space (Drew et al., 2005). Preliminary automated P-arrival times were picked using the MPX picking algorithm (Aldersons, 2004) and the automatic picks and detections were then revised manually. Around 750,000 seismograms were inspected for potential events and 27,077 P-arrivals and 14,676 S-arrivals from 1783 events were picked manually. Most events and stations are located on the mainland along the Sumatran Fault Zone (SFZ, Figure 3). Next we determined a local one dimensional (1-D) velocity model, station corrections and accurate locations simultaneously by performing a joint inversion of the picked travel times (VELEST Kissling et al., 1994) following the procedure described in Husen et al. (1999). We first inverted for a minimum RMS 1-D P-wave velocity model using a constant v_p/v_s ratio of 1.77 derived from Wadati diagrams. For this inversion we use a high quality subset of events with GAP (= largest azimuth range with no observations)≤180° and more than 10 P- and 8 S-wave observations. This procedure reduced the number of events to 588 with a total of 11,771 P- and 7,580 S-wave travel time observations. A wide range of initial P-wave velocity models (indicated in Figure 4a) was used to investigate the quality and stability of the P-wave velocity model. We then determined the minimum 1-D velocity model (black line, Figure 4a, Table ST2) by an additional series of inversions with different initial v_p/v_s ratios between 1.5 and 2.1. Due to near-vertical ray paths at shallow depths the uppermost layers down to 10 km depth are not well constrained. P velocities increase gradually from the surface and reach 7.8 km/s at 42 km depth. The velocity layers below 125 km are poorly resolved because of the reduced seismicity at greater depths.

Because of the large number of stations and events on or near the SFZ the velocity model is dominated by the crustal structure of the Sumatran mainland (Figure 3). This velocity model is not appropriate for the events in the outer forearc, so we constructed an alternative model (green line, Figure 4a, Table ST3) for the region to the northwest of the Batu Islands (box, Figure 4b) for the shallow structure ($<$30 km depth) based on an active source refraction study (Vermeesch et al., 2009), which is similar to the P-velocity model from the refraction experiment of Kieckhefer et al. (1980). Events within 150 km of the trench were located with this alternative model. Events with distances between 150 km and 250 km from the trench (labelled X–Y, Figure 5, bottom) were located in both velocity models and latitude, longitude and depth were averaged using linear interpolation. Events with distances larger than 250 km from the trench were located with the minimum 1-D velocity model. The resulting locations for both velocity models are shown in Figure SF1; the most noticeable difference between the hypocentre locations in the two models is in the region near the trench. Velocity variations in the shallow crust were accounted for by station correction terms (Figure 4b). Elevation of the land stations is taken into account explicitly, such that the station terms represent structural variations immediately below the stations. Due to computational parametrization limitations in VELEST we had to set the station elevation (depth) of the OBS stations to sea level; the corresponding travel-time compensation is accounted for by the simultaneous inversion for station correction terms (Husen et al., 1999). We estimated the average elevation related delay (0.181 s/km) and subtracted it from the nominal OBS station corrections, such that the corrected OBS station corrections plotted in Figure 4b should also represent structural variation. The majority of the station delay times are smaller than 0.5 s. Southwest of Nias four stations show significantly lower station correction terms indicating elevated P velocities, which might reflect a thin sedimentary cover or a thin crust.

In order to estimate the accuracy of the hypocentres obtained we performed jackknife tests, i.e. we randomly selected subsets of observations (picks) for stronger events (GAP≤180°) and relocated them using the final velocity model. Using reduced subsets of 20 observations per event (which is the average number of observations per event of the dataset used in the simultaneous inversion) we find an average standard deviation of 1.1 km in the horizontal direction and 2.0 km in depth. These formal errors were obtained using an 1-D velocity model which is an average of a more complex 3-D velocity structure. Although station corrections account lateral variations in the shallow subsurface the hypocentre accuracy is therefore lower than the calculated formal error for a given 1-D model. However, in areas of predominate 2-D structure (such as subduction zones) the minimum 1-D velocity model with station corrections is a good approximation of the 3-D structure (Kissling, 1988).

Local magnitudes (M_l) were calculated for all events with more than 4 amplitude readings from land stations with the formula from Hutton and Boore (1987). It was found that M_l was on average 0.25 (0.32) magnitude points less than M_w (M_b) in the Global CMT (NEIC) catalogue, respectively (Figure 6a). Although the magnitude scales use different frequency domains and are difficult to compare, one reason for the reduced M_l might be increased damping along the volcanic arc. We determined the relation between the magnitude scales using linear regression (Figure 6a):

$$\begin{aligned} M_w &= 0.90\,(\pm 0.15)\,M_l + 0.77\,(\pm 0.80) && 4.7 \leq M_l \leq 5.6 \\ M_b &= 0.68\,(\pm 0.06)\,M_l + 1.69\,(\pm 0.24) && 2.5 \leq M_l \leq 5.2 \end{aligned}$$

4. Local seismicity

The Sumatran margin shows a high level of (micro-)seismic activity. In total we located 1,783 local events in a 11 month period. For 1,220 events in the central part of the area under investigation we were able to calculate local magnitudes with magnitudes between M_l 0.8 and 5.6, of which 860 events occurred within the crust (depths ≤20 km) along the SFZ (Figure 6b). The high number of events on the mainland reflects the denser station distribution along the SFZ where the station spacing was ~15 km. In the trench-perpendicular profile (Figure 5, bottom) the seismicity defines the WBZ down to 210 km depth indicating a ~6° dip below the islands and then gradually steepening to the northeast. Linear regression of events with GAP≤180° and depths ≥80 km (projected on the trench parallel profile) yields a dip of 36(±1.5)°. Events can be spatially associated with the plate interface, the forearc, the SFZ and the WBZ. In the following we will describe the events following their distribution from northwest to southeast for the subsequent groups (see also numbers in Figure 5):

1. Plate Interface: Seismicity occurs west of Nias in a coast-parallel band of seismicity north of ~0.8°N. This band of high seismicity corresponds to the transition between regions of significant coseismic (downdip) and aseismic slip (updip) of the 2005 earthquake (Hsu et al., 2006). The band continues northwestwards, roughly following the 500 m isobath contour lines towards Simeulue Island, terminating west of Simeulue Island (Tilmann et al., 2010). Events along this band are characterized by strong scattering resulting in a smaller number of pickable S-arrivals and reduced depth accuracy. In particular, the depths of these events are very sensitive to the velocity model used (Figure SF1). Although the band terminates south of 0.8°N,

two clusters 15 km southwest of the 1984 rupture and one cluster west and adjacent to the 1935 rupture are all located close to the 500 m isobath and might represent a continuation of the seismic band at a lower seismic activity level. The hypocentral depths of the events suggest activity near the plate interface. The majority of events in the Global CMT catalogue (Figure 7) are thrust type events in this region. Southeast of Siberut Island we detected a cluster of local seismicity. This cluster was active in August 2009 with a M_w 6.7 earthquake and its aftershocks. This area (Figure 5, label ”5”) was the site of several other strong earthquakes during the last decades (Figure 7).

2. Forearc: North of the Batu Islands we observe a pronounced 10°N trending elongated cluster approximately 75×30 km in area coinciding spatially with the location of a M=7.1 earthquake in 1971 (Figure 1). The local events occur from very shallow depths in the forearc down to the plate interface at 50 km depth. The forearc southeast of this cluster between Siberut Island and the mainland shows much less activity in the shallow crust. Shallow crustal seismicity in the forearc significantly above the WBZ is also not observed in the background activity in teleseismic catalogues (e.g. Rivera et al., 2002).

3. Great Sumatran fault (SFZ): Crustal seismicity along the SFZ occurs exclusively at shallow depths less than ~20 km. The fault shows pronounced activity at 1.7°N due to an M_w 6.0 event on 19 May 2008 and its aftershocks. The crustal seismicity along the SFZ accommodates a major part of the trench-parallel component of the oblique subduction (McCaffrey et al., 2000). Between 20 km and the WBZ at 110 km depth no seismicity was

observed. We will not discuss seismicity on the SFZ further here, as this will be the focus of a separate publication.

4. Intermediate seismicity can be observed down to 210 km depth. North of the pronounced forearc cluster (Figure 5, mapview label ”2”) a streak of seismicity can be observed in the depth range between 70 km down to 170 km depth beneath the Toba caldera (Fauzi et al., 1996; Masturyono et al., 2001; Pesicek et al., 2010). On the trench-parallel profile (Figure 5, right panel) the streak is seen as an linear string of events at depths below 70 km.

5. Discussion

In order to show the spatial relation between the incoming plate structure and the observed intermediate depth seismicity we projected the prolongation of two subducted IFZ bathymetric features in Figure 8, taking into account the dip of the Australian plate. The four IFZ ridges which range from 1100 to 1900 m height at the trench, show lateral widths of 40km (IFZ1), 5 km (IFZ2), 15 km (IFZ3) and 10 km (IFZ4) (Kopp et al., 2008). For the projection we used a dip of 6° for trench distances closer than 165 km and 36° for distances greater than 165 km.

To highlight intermediate depth seismicity we removed crustal events along the SFZ in Figure 8. On the continuation of the IFZ3 a streak of seismicity is seen between 80 km and 170 km depth. It seems natural to assume that the streak of intermediate seismicity is made up of reactivated incoming fabric. The linear band of seismicity seen between Pulau Batu and the Toba caldera was first observed by Fauzi et al. (1996) who interpreted it as subducted topography of the IFZ. While this streak of intermediate seismicity is almost perfectly aligned with the prolongation of the subducted IFZ3 lineament (which is close to IFZ2 and IFZ4) on the incoming plate, the forearc cluster north of the Batu Islands is clearly offset from this lineament. Although small initial differences in the incoming plate direction have a large effect on the extrapolated trace of the IFZ features, the offset is too large to be explained by the initial subduction angle alone.

Furthermore, we observe more diffuse intermediate depth seismicity east of 99° but in which there might be two additional streaks of intermediate seismicity (red arrows, Figure 8). The region east of the subducted IFZ4 is seismically active, here ”rough” seafloor is located on the incoming oceanic plate. A seamount with basal diameter of ~35 km rising more than 3 km above the surrounding seafloor is located at 99.4°E and 4.4°S. Subduction of rough oceanic plate might explain the intermediate depth seismicity east of the subducted IFZ. Where this seamount impinges on the margin it causes frontal erosion of the lower slope (Kopp et al., 2008). The width of intermediate depth seismicity is 200 km which is in good agreement with the 210 km wide zone of rough seafloor just before the trench.

Differences between the extrapolated prolongation of the IFZ lineaments and the streaks of seismicity might be due to deformation of the subducted plate, change of plate geometry during subduction, geometrical shift of the incoming ridge chains or off-axis seamounts. The seismicity still shows the current locations of the fracture zones (and hence their topography) but the forearc region which has just been affected by the topography might extend further to the NE of the current trace of the subducted IFZ due to the NW movement of the forearc sliver. Assuming a constant rate of subduction of 57 mm/yr and a subduction length of 540 km means that the slab now at 190 km depth beneath Toba was subducted at 9.4 Ma. Intermediate depth seismicity in this depth range is generally attributed to phase transformations and dehydration embrittlement within the subducting plate or uppermost mantle (Kirby et al., 1996; Hacker et al., 2003).

The devastating Padang M_w=7.6 earthquake of 30 September 2009 occurred at 88 km depth near the eastern edge of the zone of intermediate depth seismicity. The event occurred in the lower part of the WBZ and therefore likely in the mantle lithosphere of the Australian slab (McCloskey et al., 2010). The focal mechanism appears as a slightly oblique strike-slip event aligned with the trend of the IFZ.

In the region east of the observed intermediate depth seismicity (”A” in Figure 8) the resolution of our network was sufficient to resolve intermediate depth events had they occurred. Only one intermediate depth event was registered from the region east of the subducted IFZ, where probably oceanic crust with smoother topography had been subducted. Although seismicity in the global catalogues is sparse the background seismicity from the EHB catalogue (Engdahl et al., 1998) supports the possibility of persistent downgoing streaks of seismic activity (Figure 7); the regions to the east and west of the trajectory of the subducted IFZ and the area of rough seafloor are characterised by an almost complete absence of events in the EHB catalogue. Consequently, we propose that the seismicity at depths shallower than 80 km between Pulau Batu and North Pagai is influenced by subducted IFZ fabric and rough oceanic topography.

For seismogenic depths Cloos and Shreve (1996) suggest that topographic irregularities are decapitated during subduction and the layer between the plate interfaces is filled with the rubble of sediments and sheared-off bumps. This might explain the patchy characteristics of the observed shallow (<50 km) seismicity. We suggest that the pronounced clusters of local seismicity north of the Batu Islands which ruptured in 1971 during a M=7.1 earthquake and the cluster southeast of Siberut are related to subducted fracture zone topography.

The average strike of the incoming Wharton fossil ridge is near the trench is $\sim 55^\circ$ (Deplus et al., 1998), therefore the projected trace of the subducted Wharton Ridge zone is located within the region with enhanced intermediate depth seismicity west of the Batu Islands where it presumably intersects with the trace of the IFZ. Because the orientation of this ridge is not parallel to the convergence vector the subducted Wharton Fossil Ridge might not be as obviously be reflected by intermediate depth seismicity. The parallel orientation of the convergence vector and incoming plate structures seems to favour the occurrence of reactivation of incoming (oceanic) fabric. Along the Chilean margin similar streaks of intermediate depth seismicity are found (Kirby et al., 1996; Yáñez et al., 2001): here too the convergence direction is very close to the incoming plate structures.

The offshore forearc west of Siberut Island, which is in an advanced stage of the seismic cycle, is characterised by almost aseismic behavior; only three events were detected. Also, this area shows a very low amount of seismicity in the background seismicity (Figure 7). The absence of shallow micro-seismicity beneath Siberut during the deployment reflects the locked state of the plate interface beneath Siberut, which is regarded as a seismic gap (Sieh et al., 2008). The seismic gap below Siberut Island and west offshore is bounded to the north by the subducted IFZ and the rough incoming seafloor (Figure 8).

The Batu Islands, which are located on the prolongation of the subducted IFZ, were inferred from GPS and coral data to be weakly coupled (Natawidjaja et al., 2004; Chlieh et al., 2008), although the model of (Prawirodirdjo et al., 2010) indicates that the rate of creeping might vary with time. The adjacent plate interface below Siberut Island is characterized by almost complete coupling in both models. The southern termination of the 1861 and 2005 ruptures are spatially close to the northernmost substructure of the subducted IFZ and the prolongation of the subducted IFZ1. We confirm earlier suggestions (Briggs et al., 2006; Chlieh et al., 2008) that the subducted IFZ acted as a barrier for further propagation of slip to the southeast during previous large ruptures.

The local seismicity which resolves small events during a short timescale gives good agreement with the structures that appear in the long term background seismicity. The most noticeable differences are observed in the region of the 1935 and 1984 earthquakes which showed only very small amount of activity during the 10 months of our deployment time (Figure 5). Although the forearc is seismically active northwest of the Batu Islands, the trench-parallel Mentawai fault (Figure 2, Diament et al., 1992) is not visible in the local seismicity and must therefore have a very low activity level; for the adjacent region to the southeast (Pagai Islands) the Mentawai fault was observed with local seismicity (Collings et al., 2009).

6. Conclusions

Using a dense amphibious temporary seismic network, we have characterised the seismicity of the West-Sumatran margin. Here we present locations of 1271 well constrained events, of which 586 occurred along the plate interface within the forearc crust or within the downgoing slab, and the remainder on or near the Sumatra fault. The incoming seafloor in the study region is dominated by the IFZ, which can be subdivided into four sub-ridges. This topography appears to influence seismicity at all depth intervals. At intermediate depths (80-200 km) significant seismic activity is restricted to a broad approximately 200 km wide zone, corresponding to the width of the ocean topographic anomalies such as seamounts and the subducted IFZ, but displaced some 20-30 km eastward from the projected prolongation of the IFZ along the subducted slab. Both limits to this active zone are clearly demarcated.

The western edge appears as a well-defined linear streak in map view and along-strike cross-section extending from 80-200 km depth and lying along the prolongation of IFZ3. The parallel orientation of the convergence vector and IFZ structures are suggested to favour the occurrence of reactivation of incoming (oceanic) fabric in intermediate depths. The eastern limit of the intermediate depth seismicity is less sharp; the devastating M_w=7.6 Padang earthquake of 30 September 2009 occurred near the eastern edge of this zone. At shallower depths both the forearc crust and the plate interface are characterised by enhanced seismicity levels and a few persistent clusters below the Batu Islands, which lie along the prolongation of the IFZ and are inferred to be weakly coupled (Chlieh et al., 2008).

Along the shallow plate interface seaward of the islands (or outer arc high), a different pattern of seismicity occurs in the three distinct segments within the study region, corresponding to different stages of the seismic cycle or locking behaviour. The Nias segment is in the postseismic phase after the 2005 earthquake, and aftershocks form a well-defined seismic band near the break in the forearc slope correlated with the ~500 m bathymetry contour marking the transition between the seismogenic zone and the creeping updip end of the fault. In the weakly coupled Batu segment, there is no longer a continuous band but sporadic clusters of events tend to occur near the break in forearc slope. Lastly, the Siberut segment is characterised by a nearly complete absence of events at this part of the fault interface. This segment appears to be fully locked and has not ruptured since the great 1797 earthquake ($M_w \approx 8.8$). The potential for a large event on the main plate boundary beneath Siberut Island thus remains large.

Acknowledgments

We thank the SeisUK facility in Leicester for the loan of the instruments and the continuing logistic support of this project. We acknowledge the support of the colleagues at Geotek-LIPI for this project. LIPI-EOS let us share some of the sites of the SuGaR GPS network. We thank the captain and crew of the Andalas for excellent work in the field; the landowners for hosting our stations. We thank the master and crew of R/V SONNE cruise SO-198 and SO-200 for the deployment and recovery of the OBS. The project is funded by NERC (NE/D00359/1). EOS (Earth Observatory of Singapore) we thank for supporting logistical costs of deployment on Mentawai and Batu islands. We thank the ISC and Bob Engdahl for providing the EHB Bulletin. GFZ instruments were provided by the GIPP. The Indonesian BMG and German GEOFON we thank for the station data from their permanent network. We thank A. McKittrick for compiling the the SE Asian Fault Data Base. Furthermore we thank all field crews for their excellent work under difficult conditions. Comments from two anonymous reviewers helped to further improve the manuscript. Cambridge Dep. of Earth Sci. Publication 1414.

References

Abercrombie, R. E., Antolik, M., Ekström, G., 2003. The June 2000 Mw 7.9 earthquakes south of Sumatra: Deformation in the India-Australia Plate. J. Geophys. Res. 108 (B1), 2018, doi: 10.1029/2001JB000674.

Abercrombie, R. E., Antolik, M., Felzer, K., Ekström, G., 2001. The 1994 Java tsunami earthquake: Slip over a subducting seamount. J. Geophys. Res. 106 (B4), 6595–6607.

Aldersons, F., 2004. Toward three-dimensional crustal structure of the Dead Sea region from local earthquake tomography . Ph.D. thesis, Tel Aviv University, Israel.

Barckhausen, U., SeaCause Scientific Party, 2006. The segmentation of the subduction zone offshore Sumatra: relations between upper and lower plate. EOS Trans. AGU, 87 (52), Fall Meet. Suppl., Abstract U53A-0029.

Bilek, S. L., Schwartz, S. Y., DeShon, H. R., 2003. Control of seafloor roughness on earthquake rupture behavior. Geology 31 (5), 455–458.

Briggs, R. W., Sieh, K., Meltzner, A. J., Natawidjaja, D., Galetzka, J., Suwargadi, B., Hsu, Y.-J., Simons, M., Hananto, N., Suprihanto, I., Prayudi, D., Avouac, J.-P., Prawirodirdjo, L., Bock, Y., 2006. Deformation and slip along the sunda megathrust in the great 2005 Nias-Simeulue earthquake. Science 311 (5769), 1897–1901, doi: 10.1126/science.1122602.

Cande, S. C., LaBrecque, J. L., Larson, R. L., Pitman, W. C., Golovchenko, X., Haxby, W. F., 1989. Magnetic lineations of World's Ocean Basins (one chart). Amer. Ass. Petrol. Geol., Tulsa.

Chlieh, M., Avouac, J.-P., Hjorleifsdottir, V., Song, T.-R. A., Ji, C., Sieh, K., Sladen, A., Hebert, H., Prawirodirdjo, L., Bock, Y., Galetzka, J., 2007. Coseismic Slip and Afterslip of the Great Mw 9.15 Sumatra-Andaman Earthquake of 2004. Bull. Seismol. Soc. Am. 97 (1A), S152–173, doi: 10.1785/0120050631.

Chlieh, M., Avouac, J.-P., Sieh, K., Natawidjaja, D. H., Galetzka, J., 2008. Heterogeneous coupling of the Sumatran megathrust constrained by geodetic and paleogeodetic measurements. J. Geophys. Res. 113 (B05305), doi: 10.1029/2007JB004981.

Cloos, M., Shreve, R. L., 1996. Shear-zone thickness and the seismicity of chilean- and marianas-type subduction zones. Geology 24 (2), 107–110.

Collings, R., Rietbrock, A., Lange, D., Tilmann, F. J., Natawidjaja, D. H., Suwargadi, B. W., 2009. Seismicity Within the West Sumatra Subduction Zone. EOS Trans. AGU 90 (52), Fall Meet. Suppl., Abstract T23B-1927.

Deplus, C., Diament, M., Hébert, H., Bertrand, G., Dominguez, S., Dubois, J., Malod, J., Patriat, P., Pontoise, B., Sibilla, J., 1998. Direct evidence of active deformation in the eastern Indian oceanic plate. Geology 26 (2), 131–134.

Diament, M., Harjono, H., Karta, K., Deplus, C., Dahrin, D., Zen, M. T., Gérard, M., Lassal, O., Martin, A., Malod, J., 1992. Mentawai fault zone off Sumatra: A new key to the geodynamics of western Indonesia. Geology 20 (3), 259–262.

Drew, J., Leslie, D., Armstrong, P., Michaud, G., 2005. Automated Microseismic Event Detection and Location by Continuous Spatial Mapping. SPE Annual Technical Conference and Exhibition, 9-12 October 2005, Dallas, Texas. SPE 95513-PP.

Engdahl, E. R., van der Hilst, R., Buland, R., 1998. Global teleseismic earthquake relocation with improved travel times and procedures for depth determination. Bull. Seismol. Soc. Am. 88 (3), 722–743.

Fauzi, McCaffrey, R., Wark, D., Sunaryo, Haryadi, P. Y. P., 1996. Lateral variation in slab orientation beneath Toba Caldera, northern Sumatra. Geophys. Res. Lett. 5 (23), 443–446, doi: 10.1029/96GL00381.

Gahalaut, V. K., Subrahmanyam, C., Kundu, B., Catherine, J. K., Ambikapathy, A., 2010. Slow rupture in Andaman during 2004 Sumatra–Andaman earthquake: a probable consequence of subduction of 90°E ridge. Geophys. J. Int. 180 (3), doi: 10.1111/j.1365-246X.2009.04449.x.

Hacker, B. R., Peacock, S. M., Abers, G. A., Holloway, S. D., 2003. Subduction factory 2. Are intermediate-depth earthquakes in subducting slabs linked to metamorphic dehydration reactions? J. Geophys. Res. 108 (B1), doi:10.1029/2001JB001129.

Hsu, Y.-J., Simons, M., Avouac, J.-P., Galetzka, J., Sieh, K., Chlieh, M., Natawidjaja, D., Prawirodirdjo, L., Bock, Y., 2006. Frictional Afterslip Following the 2005 Nias-Simeulue Earthquake, Sumatra. Science 312 (5782), 1921–1926, doi:10.1126/science.1126960.

Husen, S., Kissling, E., Flueh, E., Asch, G., 1999. Accurate hypocentre determination in the seismogenic zone of the subducting Nazca Plate in Northern Chile using a combined on-/offshore network. Geophys. J. Int. 138 (3), 687–701, doi: 10.1046/j.1365-246x.1999.00893.x.

Hutton, L. K., Boore, D. M., 1987. The ML scale in Southern California. Bull. Seismol. Soc. Am. 77 (6), 2074–2094.

Kieckhefer, R. M., Shor Jr, G. G., Curray, J. R., Sugiarta, W., Hehuwat, F., 1980. Seismic refraction studies of the Sunda trench and forearc basin. J. Geophys. Res. 85 (B2), 863–889.

Kirby, S., Engdahl, E. R., Denlinger, R., 1996. Intermediate-Depth Intraslab Earthquakes and Arc Volcanism as Physical Expressions of Crustal and Uppermost Mantle Metamorphism in Subducting Slabs. In: Bebout, G. E., Scholl, D. W., Kirby, S. H., Platt, J. P. (Eds.), Subduction Top to Bottom. Geophysical Monograph Series. American. Geophysical Union, Washington D.C., pp. 195–214.

Kissling, E., 1988. Geotomography with local earthquake data. Rev. Geophys. 26 (4), 659–698.

Kissling, E., Ellsworth, W. L., Eberhart-Phillips, D., Kradolfer, U., 1994. Initial reference models in local earthquake tomography. J. Geophys. Res. 99 (B10), 19.635–19.646.

Kodaira, S., Takahashi, N., Nakanishi, A., Miura, S., Kaneda, Y., 2000. Subducted Seamount Imaged in the Rupture Zone of the 1946 Nankaido Earthquake. Science 289 (5476), 104–106, doi: 10.1126/science.289.5476.104.

Konca, A. O., Avouac, J.-P., Sladen, A., Meltzner, A. J., Sieh, K., Fang, P., Li, Z., Galetzka, J., Genrich, J., Chlieh, M., Natawidjaja, D. H., Bock, Y., Fielding, E. J., Ji, C., Helmberger, D. V., 2008. Partial rupture of a locked patch of the

Sumatra megathrust during the 2007 earthquake sequence. Nature 456, 631–635.

Konca, A. O., Hjorleifsdottir, V., Song, T.-R. A., Avouac, J.-P., Helmberger, D. V., Ji, C., Sieh, K., Briggs, R., Meltzner, A., 2007. Rupture Kinematics of the 2005 M_w 8.6 Nias-Simeulue Earthquake from the Joint Inversion of Seismic and Geodetic Data. Bull. Seismol. Soc. Am. 97 (1A), S307–322.

Kopp, H., Weinrebe, W., Ladage, S., Barckhausen, U., Klaeschen, D., Flueh, E. R., Gaedicke, C., Djajadihardja, Y., Grevemeyer, I., Krabbenhoeft, A., Papenberg, C., Zillmer, M., 2008. Lower slope morphology of the Sumatra trench system. Basin Research 20 (4), 519–529, doi: 10.1111/j.1365-2117.2008.00381.x.

Krüger, F., Ohrnberger, M., 2005. Tracking the rupture of the $M_w = 9.3$ Sumatra earthquake over 1,150 km at teleseismic distance. Nature 435 (7044), 937–939, doi: 10.1038/nature03696.

Masturyono, McCaffrey, R., Wark, D. A., Roecker, S. W., Fauzi, Ibrahim, G., Sukhyar, 2001. Distribution of magma beneath the Toba caldera complex, north Sumatra, Indonesia, constrained by three-dimensional P wave velocities, seismicity, and gravity data. Geochem. Geophys. Geosyst. 2 (4), doi:10.1029/2000GC000096.

McCaffrey, R., Zwick, P. C., Bock, Y., Prawirodirdjo, L., Genrich, J. F., Stevens, C. W., Puntodewo, S. S. O., Subarya, C., 2000. Strain partitioning during oblique plate convergence in northern Sumatra: Geodetic and seismologic constraints and numerical modeling. J. Geophys. Res. 105 (B12), 28.363–28.376.

McCloskey, J., Lange, D., Tilmann, F., Nalbant, S. S., Bell, A. F., Natawidjaja, D. H., Rietbrock, A., 2010. The September 2009 Padang earthquake. Nature Geoscience 3 (2), 70–71, doi: 10.1038/ngeo753.

Mochizuki, K., Yamada, T., Shinohara, M., Yamanaka, Y., Kanazawa, T., 2008. Weak Interplate Coupling by Seamounts and Repeating M~7 Earthquakes. Science 321 (5893), 1194–1197, doi: 10.1126/science.1160250.

Müller, R. D., Roest, W. R., Royer, J.-Y., Gahagan, L. M., Sclater, J. G., 1997. Digital isochrons of the world's ocean floor. J. Geophys. Res. 102 (B2), 3211–3214.

Natawidjaja, D. H., Sieh, K., Chlieh, M., Galetzka, J., Suwargadi, B. W., Cheng, H., Edwards, R. L., Avouac, J.-P., Ward, S. N., 2006. Source parameters of the great Sumatran megathrust earthquakes of 1797 and 1833 inferred from coral microatolls. J. Geophys. Res. 111 (B06403), doi:10.1029/2005JB004025.

Natawidjaja, D. H., Sieh, K., Ward, S. N., Cheng, H., Edwards, R. L., Galetzka, J., Suwargadi, B. W., 2004. Paleogeodetic records of seismic and aseismic subduction from central Sumatran microatolls, Indonesia. J. Geophys. Res. 109, B04306, doi: 10.1029/2003JB002398.

Newcomb, K. R., McCann, W. R., 1987. Seismic history and seismotectonics of the Sunda arc. J. Geophys. Res. 92 (B1), 421–439.

Park, J., Moore, G. F., Tsuru, T., Kodaira, S., Kaneda, Y., 2004. A subducted oceanic ridge influencing the Nankai megathrust earthquake rupture. Earth Plan. Sci. Lett. 217 (1-2), 77–84, doi: 10.1016/S0012-821X(03)00553-3.

Pesicek, J. D., Thurber, C. H., Zhang, H., DeShon, H. R., Engdahl, E. R., Widiyantoro, S., 2010. Teleseismic Double-Difference Relocation of Earthquakes along the Sumatra- Andaman Subduction Zone using a Three-Dimensional Model. J. Geophys. Res.Doi: 10.1029/2010JB007443, in press.

Prawirodirdjo, L., McCaffrey, R., Chadwell, C. D., Bock, Y., Subarya, C., 2010. Geodetic observations of an earthquake cycle at the Sumatra subduction zone: Role of interseismic strain segmentation. J. Geophys. Res. 115 (B03414), doi: 10.1029/2008JB006139.

Rivera, L., Sieh, K., Helmberger, D., Natawidjaja, D., 2002. A comparative study of the sumatran Subduction-Zone earthquakes of 1935 and 1984. Bull. Seismol. Soc. Am. 92 (5), 1721–1736, doi: 10.1785/0120010106.

Robinson, D. P., Das, S., Watts, A. B., 2006. Earthquake Rupture Stalled by a Subducting Fracture Zone. Science 312 (5777), 1203–1205, doi: 10.1126/science.1125771.

Scholz, C. H., Small, C., 1997. The effect of seamount subduction on seismic coupling. Geology 25 (6), 487–490.

Sieh, K., Natawidjaja, D., 2000. Neotectonics of the Sumatran fault, Indonesia. J. Geophys. Res. 105 (B12), 28,295–28,326.

Sieh, K., Natawidjaja, D. H., Meltzner, A. J., Shen, C., Cheng, H., Li, K., Suwargadi, B. W., Galetzka, J., Philibosian, B., Edwards, R. L., 2008. Earthquake Supercycles Inferred from Sea-Level Changes Recorded in the Corals of West Sumatra. Science 322 (5908), 1674–1678, doi: 10.1126/science.1163589.

Sparkes, R., Tilmann, F., Hovius, N., 2009. Subduction of high seafloor topography restricts great earthquake rupture. Geophysical Research Abstracts, Vol. 11, EGU2009-9277, EGU General Assembly Vienna 2009,.

Tilmann, F. J., Craig, T. J., Grevemeyer, I., Suwargadi, B., Kopp, H., Flueh, E., 2010. The updip seismic/aseismic transition of the Sumatra megathrust illuminated by aftershocks of the 2004 Aceh-Andaman and 2005 Nias events. Geophys. J. Int. 181 (3), 1261–1274, doi: 10.1111/j.1365-246X.2010.04597.x.

Vermeesch, P. M., Henstock, T. J., Lange, D., McNeill, L. C., Barton, P. J., Tang, G., Bull, J. M., Tilmann, F., Dean, S. M., Djajadihardja, Y., Permana, H., 2009. 3D tomographic seismic imaging of the southern rupture barrier of the great Sumatra-Andaman 2005 earthquake. Geophysical Research Abstracts, Vol. 11, EGU2009-11509, EGU General Assembly Vienna 2009.

Yáñez, G., Ranero, C., von Huene, R., Diaz, J., 2001. Magnetic anomaly interpretation across the southern central Andes (32°S-34°S): The role of the Juan Fernández Ridge in the late Tertiary evolution of the margin. J. Geophys. Res. 106 (B4), 6325–6345, doi: 10.1029/2000JB900337.

Captions:

Figure 1:

Location map showing the oblique subduction and historical earthquakes along the Sumatran margin. Arrow shows convergence rate from Natawidjaja et al. (2006). The continuous line on the land surface indicates the Great Sumatran fault (SFZ), green lines indicate crustal faults offshore (Sieh and Natawidjaja, 2000). Oceanic fracture zones shown in black (Cande et al., 1989), dashed black line indicates hypothesized fracture zone from Barckhausen and SeaCause Scientific Party (2006). Rupture zones of the great 1797 and 1833 earthquakes are based on uplift of coral micro-atolls (Natawidjaja et al., 2006). Rupture areas from the 1861, 1935 and 1984 earthquakes are given by Rivera et al. (2002). Slip distribution of 2004 earthquake from Chlieh et al. (2007). Yellow squares represent historical shallow events between 1903 and 1984 with M≥7, where the year is indicated by the number in the square (Newcomb and McCann, 1987). Green squares indicate earthquakes with M≥7 since 1985 from the NEIC catalogue. Slip distribution from the 2005 and 2007 earthquake from Konca et al. (2007, 2008). The rupture zone of the 2000 earthquake is based on high seismic aftershock activity mapped by Abercrombie et al. (2003). Sim: Simeulue; BK: Banyak Islands; Tb: Toba; N: Nias; B: Batu Islands; P: Pulau Pini; Sb: Siberut Island; Sip: Sipora; NP: North Pagai; SP: South Pagai; E: Enggano

Figure 2:

Distribution of seismic stations used in this study. Station data from the Mentawai deployment (light blue) and the GFZ deployment (pink) were only included for the stronger events to obtain better depth constraints for the deeper hypocentres in the central part of the area under investigation and for events along the SFZ just to the northwest of our network. Crustal fault systems after Sieh and Natawidjaja (2000).

Figure 3:

Spatial distribution of manually picked P and S arrivals, shown in blue and red, respectively. The majority of the seismicity occurs at crustal depths along the SFZ, resulting in a large number of picks on the mainland stations.

Figure 4:

1-D velocity models (A) and station corrections (B). A: Thick black lines indicate the minimum 1-D velocity model with the lowest RMS from the inversion using stations with at least 10 P and 8 S arrivals with GAP≤180° and is dominated by the crustal structure of the Sumatran mainland. The range of input P models is indicated by the two dashed lines. On the right, the v_p/v_s ratios are shown. The grey lines show the output models from the inversion using different v_p/v_s ratios between 1.5 and 2.1 that fit the data equally well. For depths less than 30 km the green line indicates the P velocity model which was obtained from an active seismic study (Vermeesch et al., 2009) between the Batu Islands and Nias (shown as box, bottom) and is similar to the P-velocity model from a previous refraction experiment in the same region indicated by a red line (Kieckhefer et al., 1980). At depths greater than 30 km the velocity model was merged with the minimum 1-D velocity model with a transition between 30 and 50 km. For the uppermost 50 km a v_p/v_s ratio of 1.78 was assumed. B: P-wave station corrections corresponding to the minimum 1-D velocity model. The reference station is marked with a star and only stations with more than 10 P onsets are shown. Station elevation is accounted for explicitly for the land-stations such that station corrections represent the shallow structure. However, for computational reasons the nominal depths of the OBS needed to be fixed to sea level, and the computed station delays thus also account for the elevation effect (Husen et al., 1999). The station corrections for the OBS stations shown in blue were corrected using a slowness of 0.181 s/km. Grey lines indicate the 1000, 2000 and 4000 m isobaths.

Figure 5:
Map showing 1271 local events with more than 9 P and 4 S observations in map view, trench parallel (bottom) and perpendicular (right) profiles. Map-view: The Padang 2009 earthquake and its aftershocks are shown in green (McCloskey et al., 2010). The dashed box indicates the region for events which were used for the calculation of the histogram shown in Figure 6b. Slip distributions are the same as in Figure 1. Topography according to SRTM, bathymetry from TOPEX. Grey lines indicate the 500 m isobaths. Bottom: Hypocentre locations were calculated using the model from the active seismic experiment between 0 and 150 km from the trench; for distances greater than 250 km from the trench the minimum 1-D velocity model was used. Inbetween (labelled with X and Y in the cross-section) the locations were linearly interpolated (see text for details). Numeration refers to the consecutive numbered text in Section 4.

Figure 6:
Properties of M_l. A: M_l versus M_w (M_b) from the Global CMT (NEIC) catalogue.

The lines indicate the result from linear regression of M_l and the global observations. B: Histogram of M_l for events along the SFZ (blue) and events in the WBZ and shallow forearc (red). The smallest events which could be registered along the SFZ fault have M_l 1.7 which is one less than the events in the WBZ and shallow forearc. Only events in the central part of the network indicated by the box in Figure 5 with at least 4 amplitude readings are shown.

Figure 7:

Background seismicity along the Sumatran margin from EHB catalogue (1960–2009, grey circles) and local seismicity (red circles) in map view (left) and trench-parallel profile (right). Earthquakes with $M \geq 6$ are shown with larger circles. Focal mechanisms from the Global CMT catalogue (1976–2009, $M_w \geq 5.5$) shown on the map-view only. Hypocentres from the NEIC catalogue (1985-2010, M≥7) are shown with green stars. Slip distributions as in Figure 1. The vertical, trench parallel section on the right shows the downgoing streaks of intermediate seismicity.

Figure 8:

Map showing the bathymetry (TOPEX) with the incoming oceanic plate structures and their extrapolation below the Sumatran mainland (magenta lines) using the geometry from the inclined WBZ shown in Figure 5. The strike of of the incoming Wharton fossil ridge (~55°, Deplus et al., 1998) is indicated with a green vector. Swath bathymetry from (Kopp et al., 2008) is encircled with a yellow line. To highlight intermediate depth seismicity we removed crustal events (≤25 km) along the SFZ within the dashed black box. Events without magnitude are plotted with open circles. Red arrows show the location of two further potential streaks of intermediate seismicity. The plate coupling is indicated in grey (Chlieh et al., 2008); oceanic plate ages from Müller et al. (1997), SFZ from Sieh and Natawidjaja (2000). Slip distributions as in Figure 1. Hypocentres from the NEIC catalogue (1985-2010, M≥7) are shown with green stars. In the region labelled with ”A” the resolution of the network was sufficient to resolve intermediate depth events had they occurred.

Figure 1

Click here to download Figure: fig1.eps

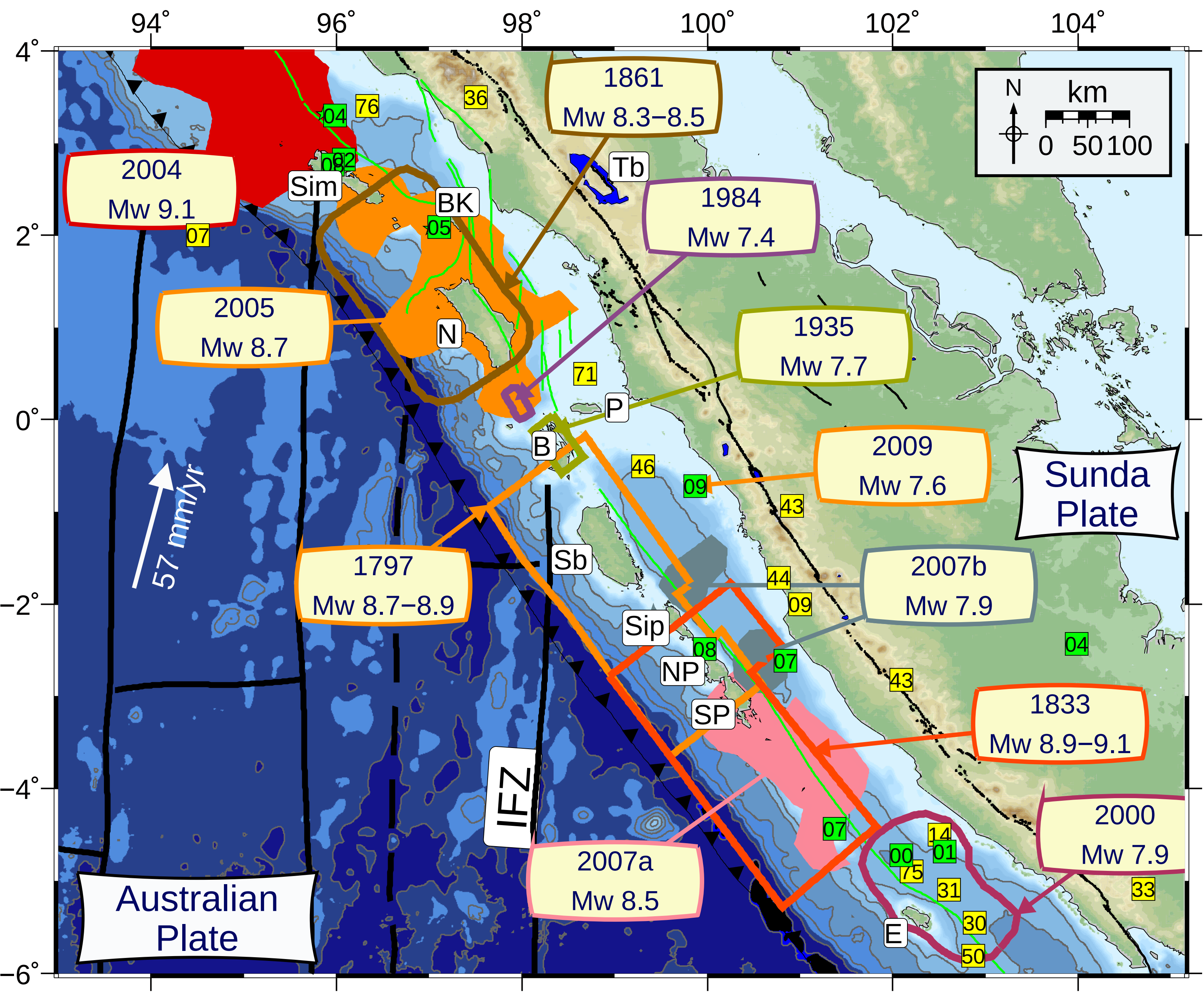

Figure 2
Click here to download Figure: fig2.eps

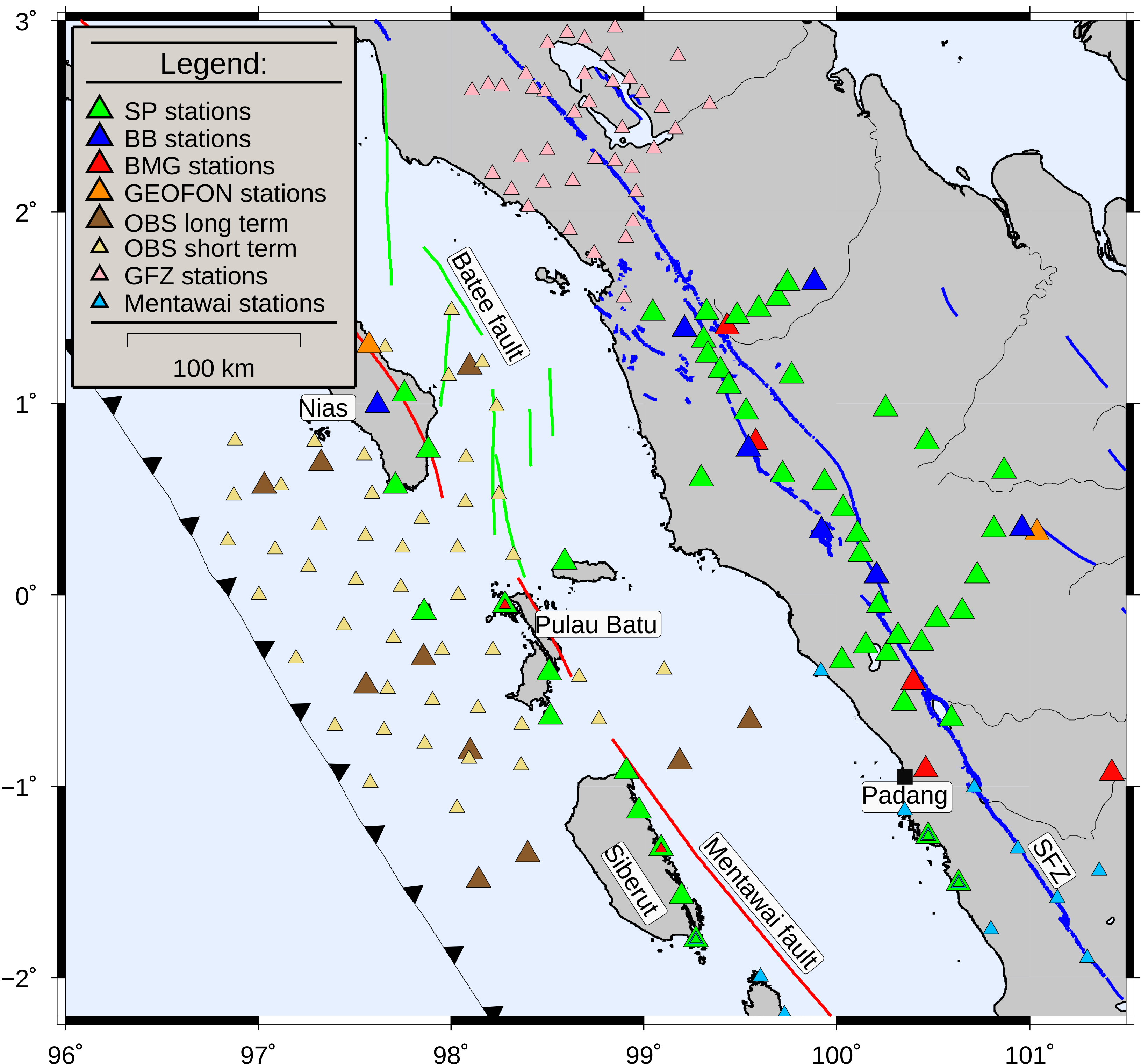

Figure 3
Click here to download Figure: fig3.eps

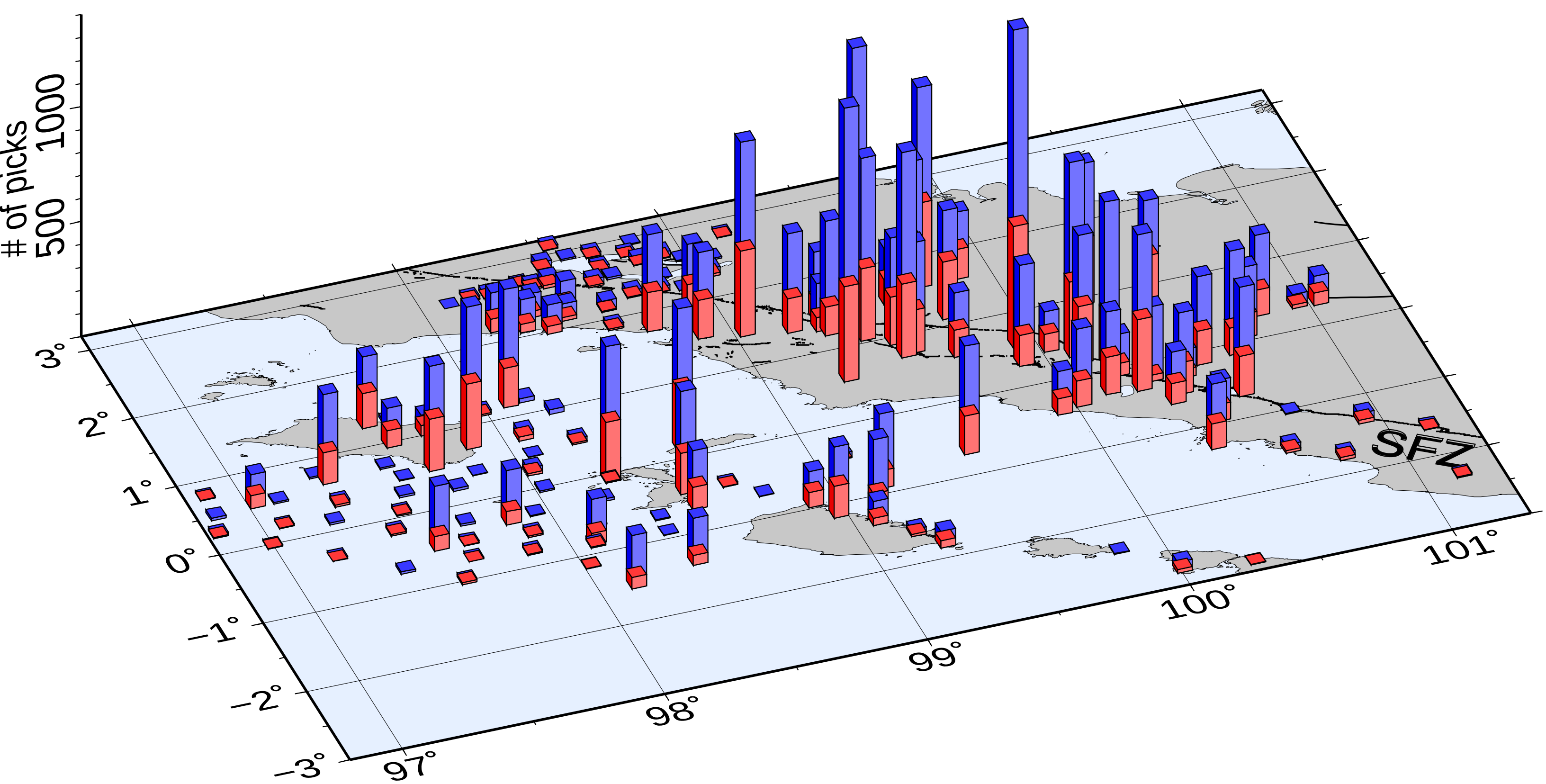

Figure 4

Click here to download Figure: fig4.eps

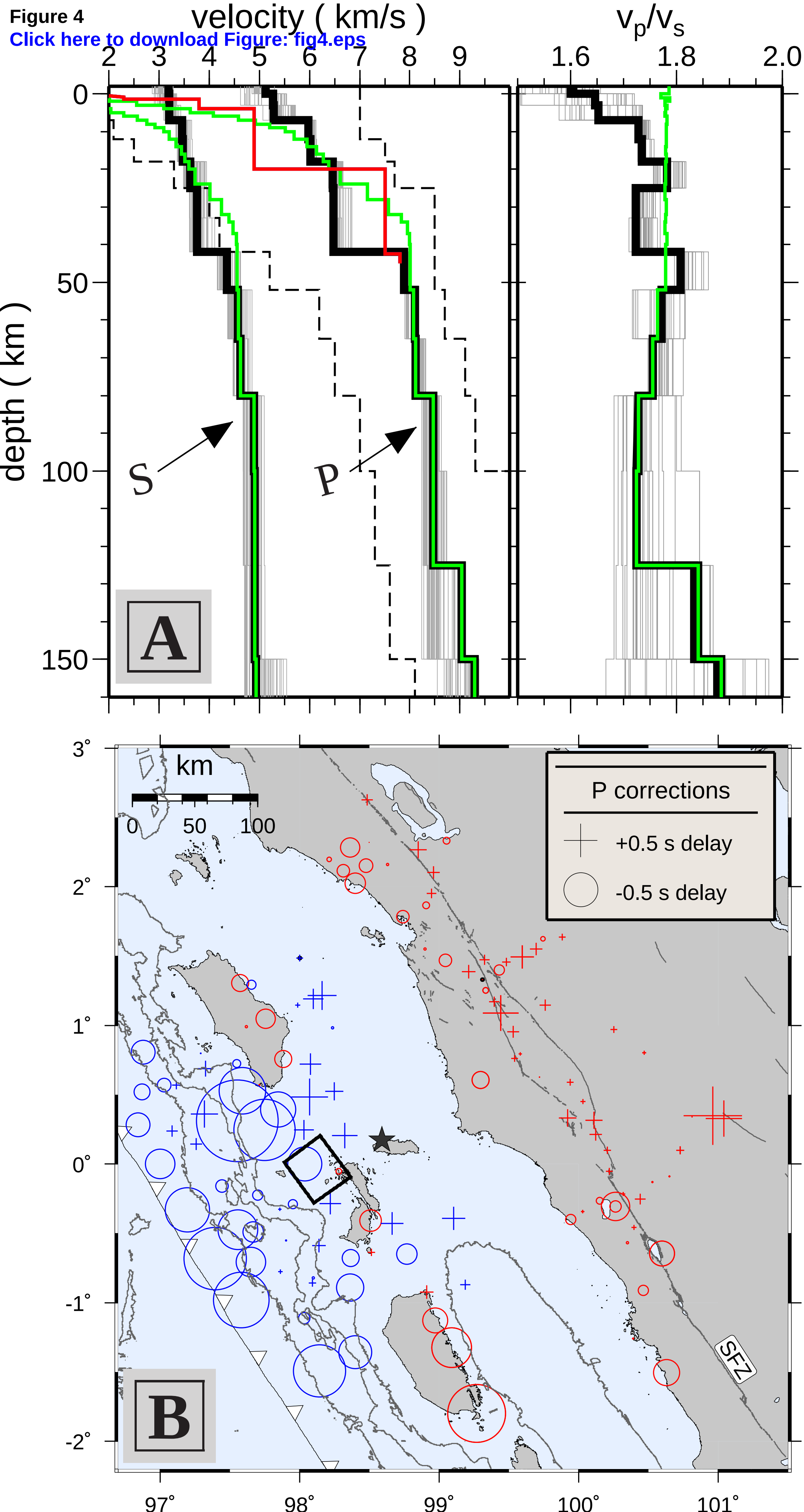

Figure 5

Click here to download Figure: fig5.eps

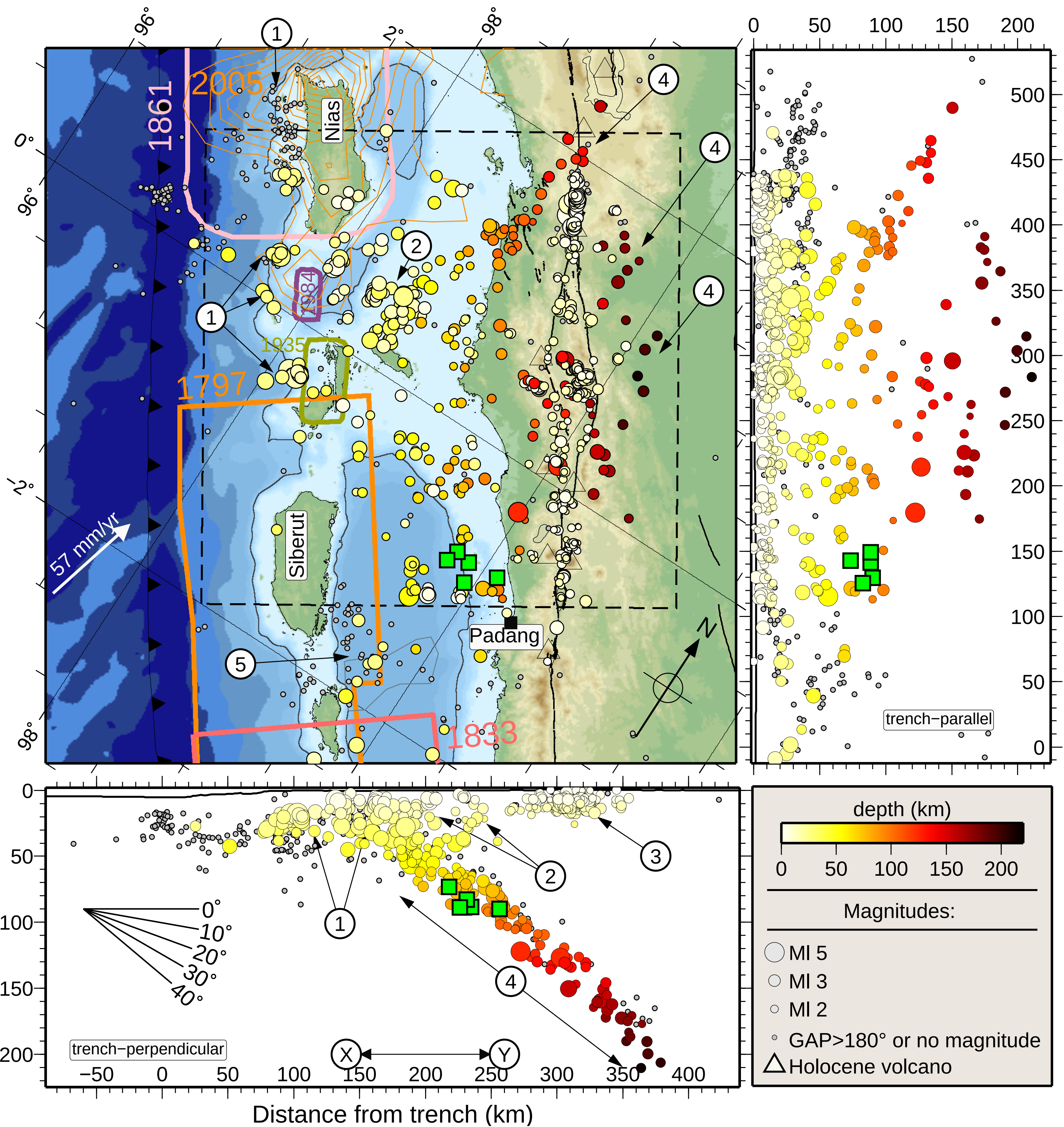

Figure 6
Click here to download Figure: fig6.eps

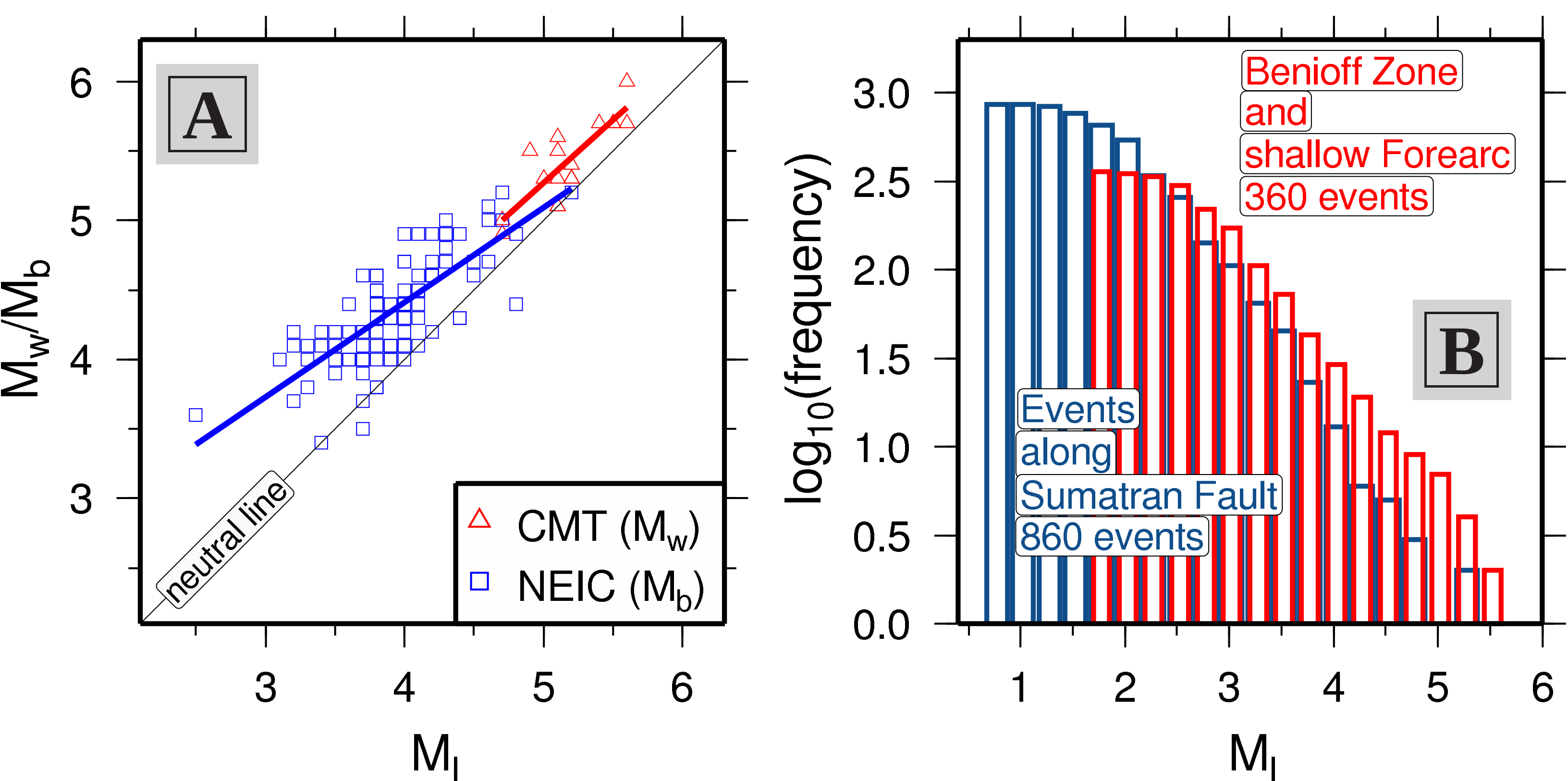

Figure 7
Click here to download Figure: fig7.eps

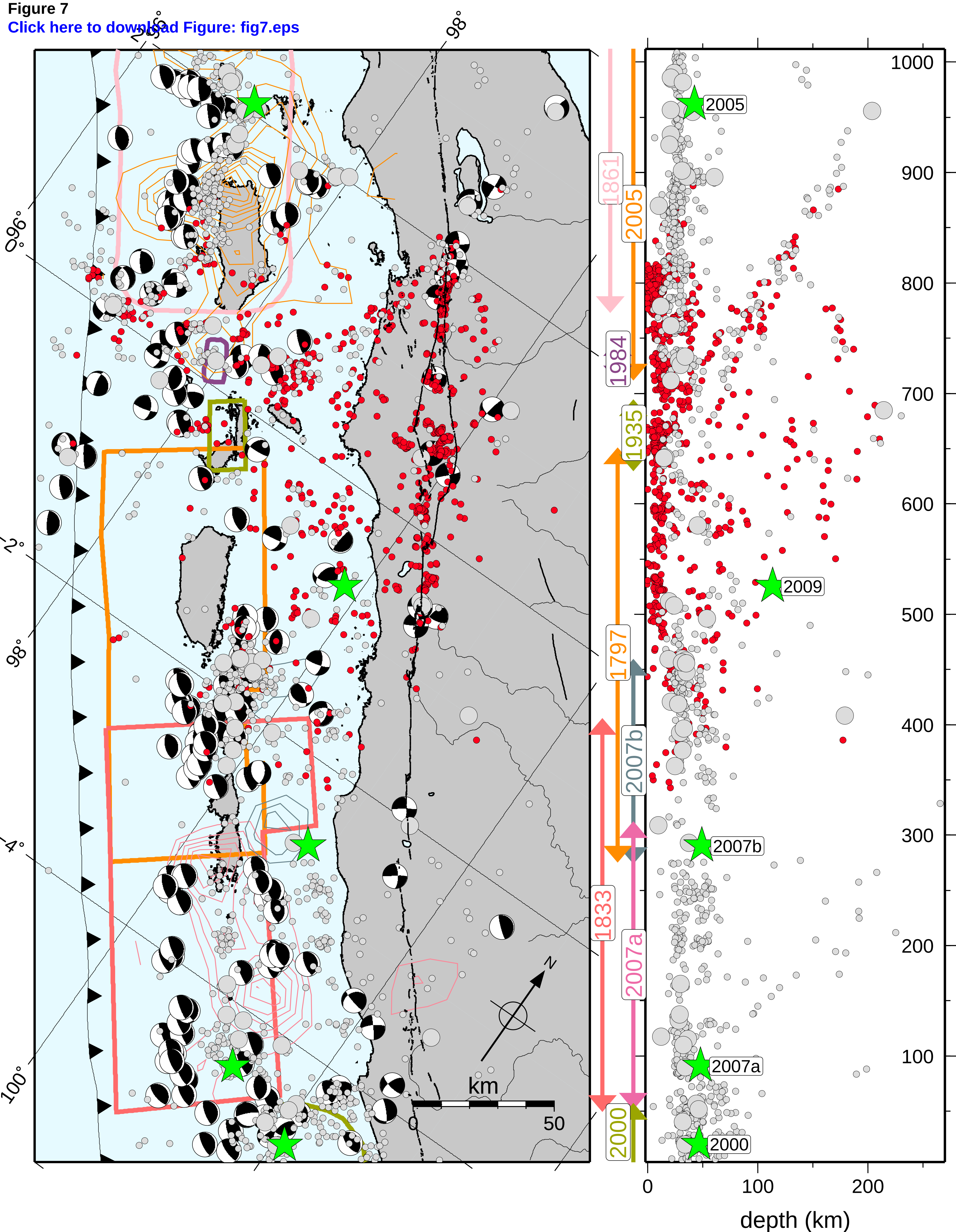

Figure 8

Click here to download Figure: fig8.eps